Available online at www.sciencedirect.com
SCIENCE DIRECT®
ELSEVIER
Physics of the Earth and Planetary Interiors 150 (2005) 29–43
PHYSICS OF THE EARTH AND PLANETARY INTERIORS
www.elsevier.com/locate/pepi

Three-dimensional nonlinear regularized inversion of the induced polarization data based on the Cole–Cole model

Ken Yoshioka, Michael S. Zhdanov *

University of Utah, Department of Geology and Geophysics, Salt Lake City, UT 84112, USA

Received 28 January 2003; received in revised form 30 October 2003; accepted 16 August 2004

Abstract

The quantitative interpretation of induced polarization (IP) data in a complex three-dimensional (3D) environment is a very challenging problem. The analysis of IP phenomena is usually based on models with frequency dependent conductivity distributions. In this paper, we develop a technique for 3D nonlinear inversion of IP data based on the Cole–Cole relaxation model. Our method takes into account, though in an approximate way, the nonlinearity of electromagnetic induction and IP phenomena, and inverts the observed data for the Cole–Cole model parameters. The solution of the 3D IP inverse problem is based on both smooth and focusing regularized inversion, which helps to generate more reliable images of the subsurface structures. The method is tested on synthetic models with anomalous conductivity and intrinsic chargeability, and is also applied to a practical 3D IP survey. We demonstrate that both the electrical conductivity and the chargeability distributions, as well as the other parameters of the Cole–Cole model, can be recovered from the observed IP data simultaneously. The recovered parameters of the Cole–Cole model can be used for the discrimination of the different types of mineralization, which is an important goal in mineral exploration.

Keywords: Induced polrarization; Three-dimensional; Inversion; Cole–Cole model

1. Introduction

The electromagnetic data observed in geophysical surveys, in general case, reflect two phenomena: (1) electromagnetic induction (EMI) in the earth, and (2) IP effects related to the relaxation of polarized charges in rock formations. The EMI effect can be simulated by the solution of electromagnetic (EM) field equations in the geoelectrical model characterized by frequency independent conductivity. The analysis of IP phenomena is usually based on models with frequency dependent conductivity distribution. One of the most popular is the Cole–Cole relaxation model (Cole and Cole, 1941) analyzed in the pioneering work of Pelton (1977). This model has been used in a number of more recent publications for the interpretation of IP data (see, for example, Yuval and Oldenburg, 1997; Routh and Oldenburg,

* Corresponding author. Present address: University of Utah, Department of Geology and Geophysics, 135 S. 1460 E., Rm 719, 84112, Utah, U.S.A. Tel.: +1 801 581 7750; fax: +1 801 581 7065.
E-mail address: mzhdanov@mines.utah.edu (M.S. Zhdanov).

0031-9201/$ – see front matter © 2004 Published by Elsevier B.V.
doi:10.1016/j.pepi.2004.08.034

1998). The parameters of the conductivity relaxation model can be used for discrimination of the different types of rock formations, which is an important goal in mineral exploration.

The quantitative interpretation of IP data in a complex three-dimensional (3D) environment is a very challenging problem because it is complicated by coupling with the electromagnetic induction effects. This problem was considered in the paper by Li and Oldenburg (2000), where the authors presented an algorithm based upon a linearized expression for the IP response. However, linearized inversion ignores those nonlinear effects, which are significant in IP phenomena. It is difficult to use a linearized approach to recover Cole–Cole model parameters.

In this paper, we develop a technique for three-dimensional nonlinear inversion of IP data based on the Cole–Cole relaxation model. Our method takes into account, though in an approximate way, the nonlinear nature of both electromagnetic induction and IP phenomena, and inverts the data for the Cole–Cole model parameters. These parameters may be used to separate the responses from the different types of mineralization. In their pioneering paper, Zonge and Wynn (1975) wrote that "the only electrical method which shows promise of providing discriminatory capabilities is the low-frequency complex resistivity spectra technique." Almost thirty years later, we should say that this statement is still correct. However, in spite of increased number of publications for interpretation of IP data, we still do not have an appropriate tool for the reliable 3D inversion of spectral IP data with respect to the relaxation model parameters.

Another goal of this paper is to develop a technique for nonlinear inversion of IP data, which can be applied to multi-transmitter data sets. The main difficulty with multi-transmitter data inversion is that, in principle, this observation system requires significantly more time for modeling and inversion of the observed data than, for example, a fixed transmitter system. Recently, Zhdanov and Tartaras (2002) developed a new technique, which allows for the modeling and inversion of multi-transmitter data simultaneously for all transmitter positions. This technique is based on the so-called localized quasi-linear (LQL) approximation. In this paper we use the localized quasi-linear (LQL) method for 3D inversion of IP data in the frequency domain. We apply the integral equation (IE) method for 3D forward modeling (Xiong, 1992) of a synthetic data set, and the LQL approximation method for 3D inversion. The solution of the 3D IP inverse problem is based on both smooth and focusing regularized inversion (Zhdanov, 2002), which helps generate more reliable images of the subsurface structures. The method is tested on synthetic models with anomalous conductivity and intrinsic chargeability. We demonstrate that both the electrical conductivity and the chargeability distributions, as well as the other parameters of the Cole–Cole model can be recovered from the observed IP data simultaneously. The recovered parameters of the Cole–Cole model can be used for the discrimination of the different rock. The method was also applied to practical 3D IP survey data, collected by Rio Tinto Mining and Exploration.

2. Forward modeling of induced polarization based on the LQL approximation and the Cole–Cole model

The quasi-linear (QL) approximation is based on an assumption that the anomalous electric field $\mathbf{E}^{\mathrm{a}}$ inside the inhomogeneous domain is linearly proportional to the background field $\mathbf{E}^{\mathrm{b}}$ through the electrical reflectivity tensor $\hat{\lambda}$ (Zhdanov and Fang, 1996a, 1996b):

$$\mathbf{E}^{\mathrm{a}}(\mathbf{r}) \approx \hat{\lambda}(\mathbf{r})\mathbf{E}^{\mathrm{b}}(\mathbf{r}) \tag{1}$$

Substituting formula (1) into the known integral representations for the anomalous electric and magnetic fields, $\mathbf{E}^{\mathrm{a}}$, $\mathbf{H}^{\mathrm{a}}$ (Hohmann, 1975; Weidelt, 1975), we obtain the QL approximations $\mathbf{E}^{\mathrm{a}}_{\mathrm{QL}}(\mathbf{r})$ and $\mathbf{H}^{\mathrm{a}}_{\mathrm{QL}}$ for the anomalous electric and magnetic fields in the frequency domain:

$$\mathbf{E}^{\mathrm{a}}_{\mathrm{QL}}(\mathbf{r}) = \int_D \hat{\mathbf{G}}_{\mathrm{E}}(\mathbf{r}_j|\mathbf{r})\Delta\sigma(\mathbf{r})(\hat{\mathbf{I}} + \hat{\lambda}(\mathbf{r}))\mathbf{E}^{\mathrm{b}}(\mathbf{r})\,\mathrm{d}v = \mathbf{G}_{\mathrm{E}}(\Delta\sigma(\hat{\mathbf{I}} + \hat{\lambda}(\mathbf{r}))\mathbf{E}^{\mathrm{b}}(\mathbf{r})) \tag{2}$$

$$\mathbf{H}^{\mathrm{a}}_{\mathrm{QL}}(\mathbf{r}_j) = \int_D \hat{\mathbf{G}}_{\mathrm{H}}(\mathbf{r}_j|\mathbf{r})\Delta\sigma(\mathbf{r})(\hat{\mathbf{I}} + \hat{\lambda}(\mathbf{r}))\mathbf{E}^{\mathrm{b}}(\mathbf{r})\,\mathrm{d}v = \boldsymbol{G}_{\mathrm{H}}(\Delta\sigma(\hat{\mathbf{I}} + \hat{\lambda}(\mathbf{r}))\mathbf{E}^{\mathrm{b}}(\mathbf{r})) \tag{3}$$

where $\hat{\mathbf{G}}_{\mathrm{E}}(\mathbf{r}_j|\mathbf{r})$ and $\hat{\mathbf{G}}_{\mathrm{H}}(\mathbf{r}_j|\mathbf{r})$ are the electric and magnetic Green's tensors defined for an unbounded conductive medium with the background conductivity σ_b; D denotes a domain with the anomalous conductivity distribution $\Delta\sigma$; $\mathbf{G}_E$ and $\mathbf{G}_H$ are the corresponding Green's linear operators.

Note that the electrical reflectivity tensor $\hat{\lambda}$, in the general case, depends on the illuminating background field $\mathbf{E}^b$. In the case of the localized quasi-linear (LQL) approximation (Zhdanov and Tartaras, 2002), we assume that the electrical reflectivity tensor $\hat{\lambda}_L$ is source independent. The expressions (2) and (3) with the localized $\hat{\lambda}_L$ are called *the localized quasi-linear* (LQL) *approximations*.

Note that in the LQL approximation one can choose different types of reflectivity tensors. For example, we can introduce a scalar reflectivity coefficient. In this case, we have $\hat{\lambda}_L = \lambda_L \hat{\mathbf{I}}$ (Zhdanov and Tartaras, 2002), and:

$$\mathbf{E}^a(\mathbf{r}) \approx \lambda_L(\mathbf{r})\mathbf{E}^b(\mathbf{r}) \tag{4}$$

Substituting formula (4) into Eqs. (2) and (3), we obtain the scalar LQL approximations $\mathbf{E}^a_{LQL}$ and $\mathbf{H}^a_{LQL}$ for the anomalous fields.

We can use the LQL approximation for 3D modeling of both electromagnetic induction and IP effects in inhomogeneous structures. In this case, formulae (2) and (3) should be modified to take into account the IP effect. The main modification involves the expression for the anomalous conductivity, $\Delta\sigma$, which should be substituted now by complex value, $\Delta\tilde{\sigma}$. In order to take into account IP effect, one should assume that the conductivity within the anomalous domain, $\sigma_b + \Delta\tilde{\sigma}$, becomes complex and frequency dependent:

$$\sigma_b + \Delta\tilde{\sigma} = \sigma(\omega) = \frac{1}{\rho(\omega)} \tag{5}$$

We consider that the complex resistivity, $\rho(\omega)$, is described by the well known Cole–Cole relaxation model (Cole and Cole, 1941), given by:

$$\rho(\omega) = \rho\left(1 - \eta\left(1 - \frac{1}{1 + (i\omega\tau)^C}\right)\right) \tag{6}$$

where ρ is the dc resistivity (Ω m); ω the angular frequency (rad/s); τ the time constant (s); η the intrinsic chargeability (Seigel, 1959); C the relaxation parameter. The dimensionless intrinsic chargeability, η, which varies from 0 to 1, characterizes the intensity of the IP effect.

In this case, the anomalous conductivity, $\Delta\tilde{\sigma}$, is expressed as

$$\Delta\tilde{\sigma} = \sigma(\omega) - \sigma_b$$

$$= \sigma\left(1 - \eta\left(1 - \frac{1}{1 + (i\omega\tau)^C}\right)\right)^{-1} - \sigma_b \tag{7}$$

where $\sigma = 1/\rho$.

Substituting Eq. (7) into formula (2), we obtain the corresponding LQL approximations for the IP anomalous electric field

$$\mathbf{E}^a_{LQL}(\mathbf{r}_j) = \mathbf{G}_E(\Delta\tilde{\sigma}(1 + \lambda_L(\mathbf{r}))\mathbf{E}^b(\mathbf{r})) \tag{8}$$

where $\mathbf{r}_j$ is an observation point, and $\mathbf{r}$ is a point within domain D.

3. Inversion based on the LQL approximation and the Cole–Cole model

Following Zhdanov and Fang (1999) and Zhdanov and Tartaras (2002), we introduce a new function,

$$m(\mathbf{r}) = \Delta\tilde{\sigma}(\mathbf{r})(1 + \lambda_L(\mathbf{r})) \tag{9}$$

which we call a modified material property parameter and is frequency dependent. Eqs. (2) and (3) now take the form:

$$\mathbf{E}^a_{LQLi}(\mathbf{r}_j) = \mathbf{G}_E(m(\mathbf{r})\mathbf{E}^b_i(\mathbf{r})) \tag{10}$$

$$\mathbf{H}^a_{LQLi}(\mathbf{r}_j) = \mathbf{G}_H(m(\mathbf{r})\mathbf{E}^b_i(\mathbf{r})) \tag{11}$$

where i is the index of the corresponding transmitter, assuming that we have the multi-transmitter survey. We assume now that the anomalous parts of the electric $\mathbf{E}^a_i(\mathbf{r}_j)$, and/or magnetic $\mathbf{H}^a_i(\mathbf{r}_j)$, fields are measured in the number of observation points, $\mathbf{r}_j$. Using the LQL approximation for the observed fields, $\mathbf{d}_i$ we arrive at the following equation:

$$\mathbf{d}_i(\mathbf{r}_j) = \mathbf{G}_d(m(\mathbf{r})\mathbf{E}^b_i(\mathbf{r})) \tag{12}$$

which is linear with respect to the material property parameter $m(\mathbf{r})$. In equation (12), $\mathbf{d}_i$ represents either the electric $\mathbf{E}$, or magnetic $\mathbf{H}$ field, generated by the transmitter with the index i, and $\mathbf{G}_d$ denotes the Greens operator $\mathbf{G}_E$ or $\mathbf{G}_H$ correspondingly. Note that, in the framework of this formulation, we assume that the background conductivity is known. In practice it can be determined from additional geophysical information, or by averaging the results of dc resistivity soundings over the area of investigation.

Eq. (12) is called a *material property equation*. We numerically solve this linear equation using the re-weighted regularized conjugate (RRCG) method described in Zhdanov (2002). This method employs both the smooth and focusing regularized inversion, which helps to generate more reliable images of the subsurface structures (Zhdanov, 2002).

Substituting formulae (9) and (4) into (10), and by taking an average of each side of Eq. (10) over all transmitter indices, we find:

$$\lambda_L(\mathbf{r})\tilde{\mathbf{E}}^b(\mathbf{r}) = \mathbf{G}_E(m(\mathbf{r})\tilde{\mathbf{E}}^b(\mathbf{r})) \tag{13}$$

where

$$\tilde{\mathbf{E}}^b(\mathbf{r}) = \frac{1}{N}\sum_{i=1}^{N}\mathbf{E}_i^b(\mathbf{r}) \tag{14}$$

Note that, in the original paper on the LQL approximation by Zhdanov and Tartaras (2002), they omitted an average background field $\tilde{\mathbf{E}}_b$ in the expression for λ_L. The corresponding simplified formula for λ_L provided an accurate enough approximation for airborne data because the transmitter was located above the ground, and they observed only inductive excitation of the geoelectrical structures. In an IP survey, the sources (electric dipoles) are located on the ground. In this case we are dealing with the galvanic excitation, which we found requires a more accurate formula for computing λ_L. After solving equation (12), we determine λ_L, $(\mathbf{r})$ from formula (13). Knowing $\lambda_L(\mathbf{r})$ and $m(\mathbf{r})$, we can find $\Delta\tilde{\sigma}(\mathbf{r})$ $(\mathbf{r})$ from Eq. (9).

Note that Eq. (9) holds for any frequency, because the electrical reflectivity coefficient and the material property parameter are the functions of frequency as well: $\lambda_L = \lambda_L(\mathbf{r}, \omega)$, $m = m(\mathbf{r}, \omega)$. We assume also that in formula (7), the parameters $\sigma = \sigma(\mathbf{r})$, $\eta = \eta(\mathbf{r})$, $\tau = \tau(\mathbf{r})$, and $C = C(\mathbf{r})$ vary within the anomalous domain:

$$\Delta\tilde{\sigma}(\mathbf{r}, \omega) = \sigma(\mathbf{r})(1 - \eta(\mathbf{r}) \times \left(1 - \frac{1}{1 + (i\omega\tau(\mathbf{r}))^{C(\mathbf{r})}}\right)\Bigg)^{-1} - \sigma_b \tag{15}$$

Therefore, the parameters $\sigma(\mathbf{r})$, $\eta(\mathbf{r})$, $\tau(\mathbf{r})$, and $C(\mathbf{r})$ of the complex conductivity $\Delta\tilde{\sigma}(\mathbf{r}, \omega)$ can be found by using the least square method of solving Eq. (9) at each point $\mathbf{r}$ inside the area of inversion:

$$||m(\mathbf{r}, \omega) - \Delta\tilde{\sigma}(\mathbf{r}, \omega)(1 + \lambda_L(\mathbf{r}, \omega))||_{L_2(\omega)} = \min \tag{16}$$

The dc resistivity $\rho(\mathbf{r})$ is then determined as the inverse of the dc conductivity: $\rho(\mathbf{r}) = 1/\sigma(\mathbf{r})$.

Note in the conclusion of this section that, in spite of the fact that the LQL approximation reduces the inverse problem to the linear equation (12), it still takes into account the nonlinear effects in EM data. This can be seen from Eq. (9) for material property parameter. It depends on the product of the anomalous conductivity $\Delta\tilde{\sigma}$, and the reflectivity coefficient λ_L, while λ_L itself is a function of the anomalous conductivity $\Delta\tilde{\sigma}$, as well. This is why the LQL method actually provides for a nonlinear inversion of IP data.

4. Numerical modeling results

We generated the synthetic EM data for the typical geoelectrical models of the conductive or resistive targets within a homogeneous background.

The electromagnetic field in the models is generated by electric dipole transmitters with a length of $a = 50$ m (galvanic EM field excitation) and is measured by electric dipole receivers of the same length. The transmitters and receivers are positioned along a set of profiles. For each transmitter position, we have up to six receivers located at the distances of na from the end of the dipole transmitter, where $n = 1, 2, \ldots, 6$, respectively. Altogether we have 13 transmitters in each profile of 600 m length. For the transmitters located at the right hand side of the profile, the number of the corresponding receivers is reduced respectively, as shown in Fig. 1 (top panel), so that for the transmitter number 11, we have just one receiver.

The transmitters and the receivers are located along thirteen profiles, A, B, C, ..., M, deployed in the y-direction with 50 m separation (Fig. 1, bottom panel). The dots denote the centers of the transmitter and receiver dipoles, respectively. The total number of receivers is 169.

Model 1 consists of two cubic conductive and resistive bodies in a 100 Ω m homogeneous background (Fig. 2). The IP parameters of the conductive body de-

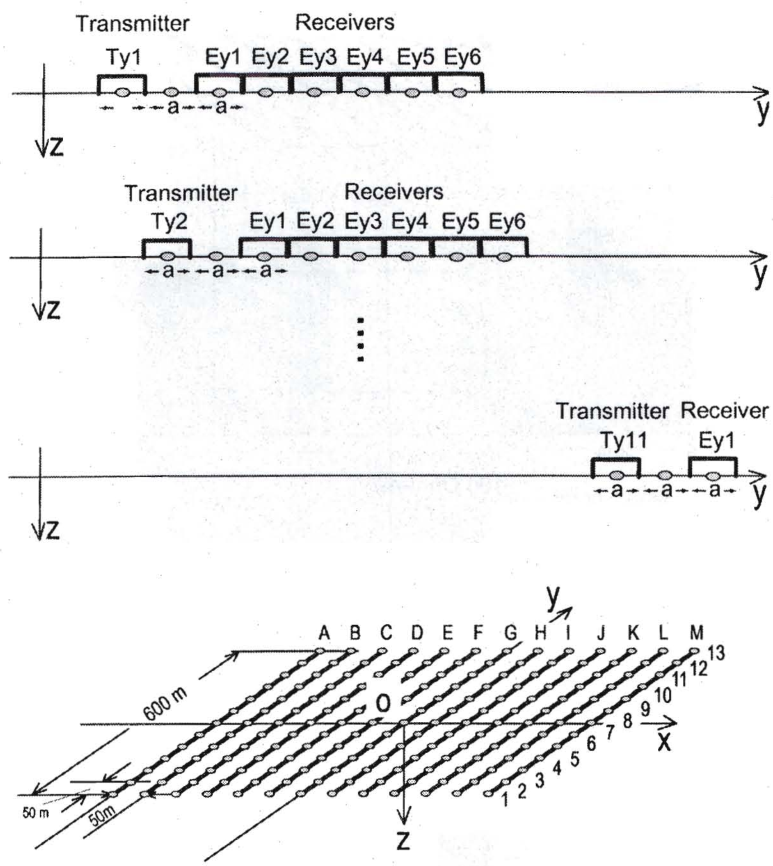

Fig. 1. Sketch of a typical electrical dipole–dipole IP survey. For each transmitter position we have up to six receivers located at the distances of *n*a from the end of the bipole transmitter, where $n = 1, 2, \ldots, 6$, respectively (top panel). The transmitters and the receivers are located along thirteen profiles, A, B, C, . . ., M, deployed in the *y*-direction with 50 m separation (bottom panel). The dots denote the centers of the transmitter and receiver dipoles, respectively. The total number of receivers is 143.

fined by the Cole–Cole relaxation model are as follows:

$$\begin{aligned} \rho &= 10\,\Omega\,\mathrm{m} \\ \tau &= 0.01\,\mathrm{s} \\ \eta &= 0.5 \\ \mathrm{C} &= 0.8 \end{aligned} \tag{17}$$

while the parameters of the resistive body are:

$$\begin{aligned} \rho &= 1000\,\Omega\,\mathrm{m} \\ \tau &= 0.01\,\mathrm{s} \\ \eta &= 0.5 \\ \mathrm{C} &= 0.8 \end{aligned} \tag{18}$$

The top of the bodies are located at a depth of 100 m. The cubic body sides have a length of 150 m.

The synthetic EM data for this model were generated using the integral equation forward modeling code SYSEM (Xiong, 1992). We used seven frequencies: 0.5, 1, 2, 4, 8, 16, and 32 Hz. The real and imaginary parts of the synthetic observed data were contaminated by 2% Gaussian noise and inverted using focusing regularized LQL inversion. The parameters $\tau = 0.01$ s and $C = 0.8$ of the Cole–Cole model were fixed, and the inversion was run for the dc resistivity and the intrinsic chargeability.

The area of inversion was subdivided into 1352 cubic cells ($13 \times 13 \times 8$ in the *x*, *y*, and *z*-directions, respectively), with the size of each cubic cell 50 m. Figs. 3 and 4 present the cross-sections of the reconstructed resistivity and chargeability along the lines passing over two bodies (perpendicular to the obser-

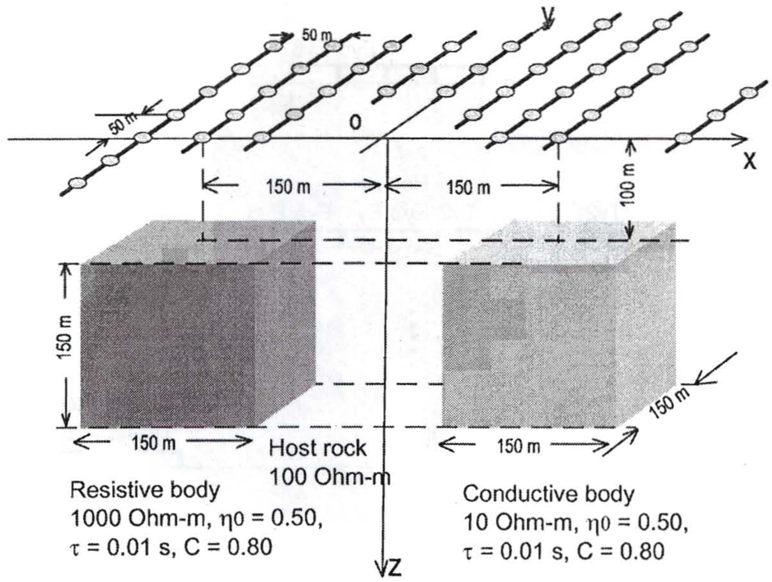

Fig. 2. Model 1 of two rectangular conductive and resistive bodies in a 100 Ωm homogeneous background.

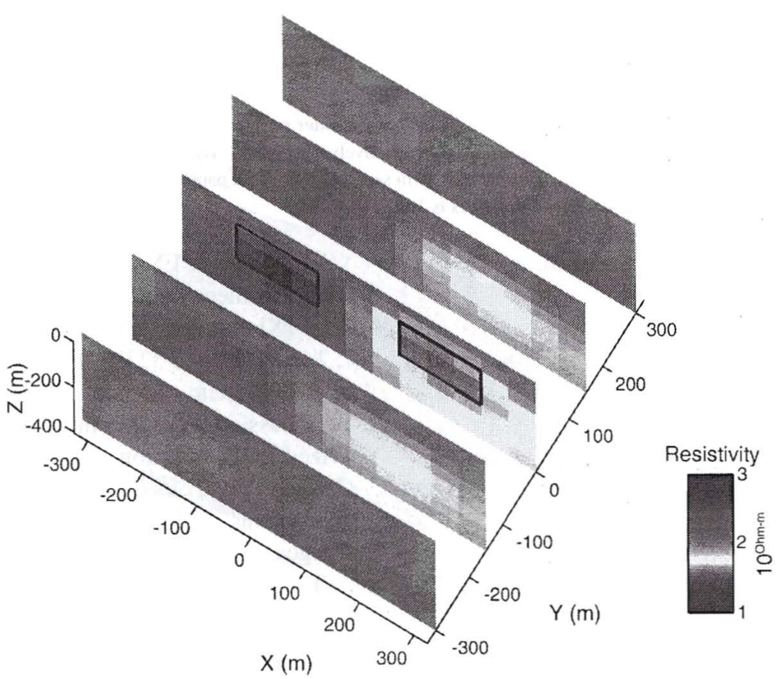

Fig. 3. The resistivity distribution obtained by inversion of the IP data for model 1. The vertical cross sections are perpendicular to the observational profiles. The solid lines outline the true position of the bodies.

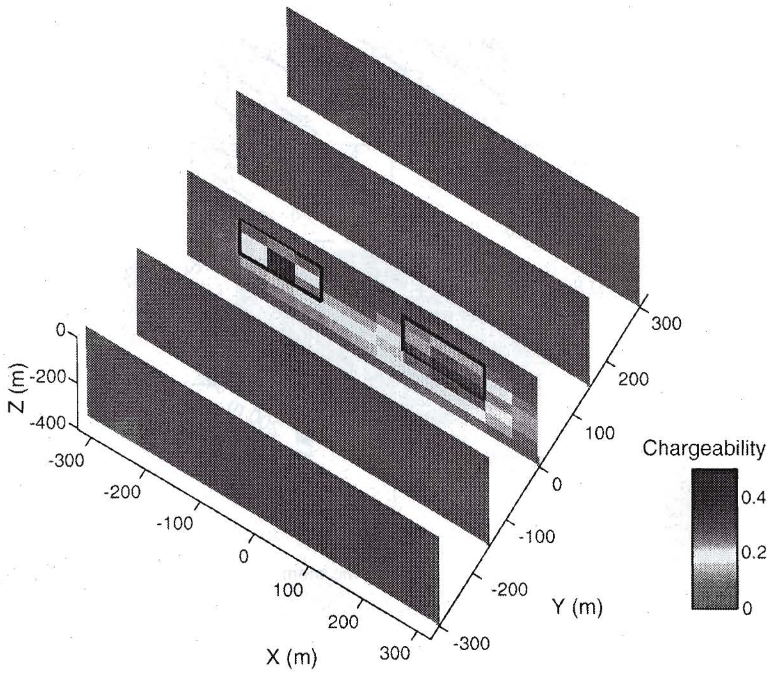

Fig. 4. The chargeability distribution obtained by inversion of the IP data for model 1. The vertical cross sections are perpendicular to the observational profiles. The solid lines outline the true position of the bodies.

vational profiles). One can see that the focusing regularized inversion produces a good image of both the conductivity and chargeability distributions.

Model 2 represents the conductive dipping dike with the upper part containing the anomalous chargeability, in a $100\,\Omega\,\mathrm{m}$ homogeneous background (Fig. 5). The chargeability of the upper part of the dike is defined by the Cole–Cole model with the following parameters:

$$\begin{aligned}\rho &= 10\,\Omega\,\mathrm{m}\\ \tau &= 0.01\,\mathrm{s}\\ \eta &= 0.5\\ C &= 0.8\end{aligned} \tag{19}$$

The lower part of the dike has a conductivity of $10\,\Omega\,\mathrm{m}$ but produces no IP Geffect. The geometry of the observation system is the same as in model 1, and the EM field in this model is generated using the same electric dipoles, as in model 1. The synthetic data for this model were also computed using the integral equation forward modeling code SYSEM (Xiong, 1992). The data were contaminated by 2% Gaussian noise and inverted using focusing regularized LQL inversion. We use the same grid for inversion as for model 1.

Figs. 6 and 7 present the results of the inversion for model 2. The bold black lines in these figures outline the location of the dipping dike with the IP effect, while the thin black lines outline the conductive part without an IP effect. We can see the location of the conductive target outlined by the bold and thin black lines in the images of resistivity, and the location of the chargeability outlined only by the bold black lines in the images of chargeability. The resistivity and intrinsic chargeability are recovered quite correctly for this complicated model.

In order to check the accuracy of the LQL approximation in modeling and inversion of the IP data, we computed the theoretical response for the model of the dike obtained by LQL inversion using the rigorous IE forward modeling code SYSEM (Xiong, 1992). Fig. 8 presents a comparison between the observed and predicted data along three profiles passing over the dike. We show in this figure the real part of the observed

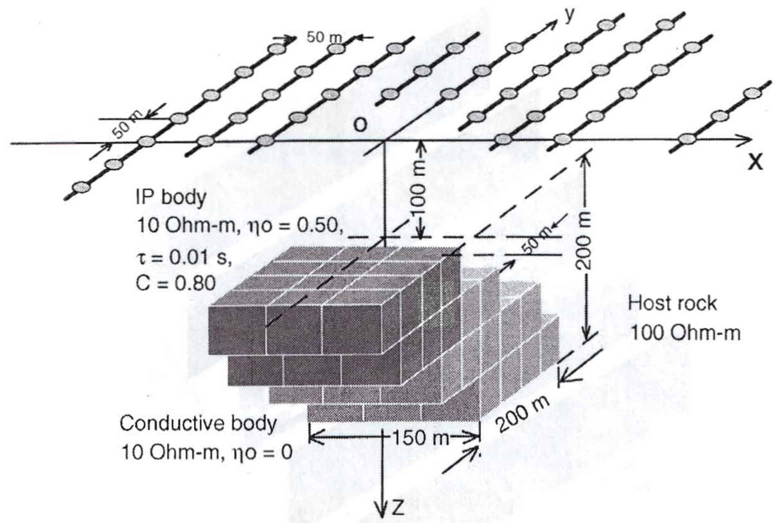

Fig. 5. Model 2 of a conductive dipping dike with the upper part containing the anomalous chargeability in a 100 Ω m homogeneous background.

electric field at a frequency of 4 Hz in the receivers located at the distances of na from the end of the dipole transmitter, respectively, where $n = 3$, 5, and $a = 50$ m. We present the comparison for the real part only, because the imaginary parts of the electric field are two orders of magnitude smaller than the real parts and do not effect the inversion result. One can see in Fig. 8 that the observed and predicted data computed using the rigorous forward modeling code are very close to each other. The misfit between two data sets increases

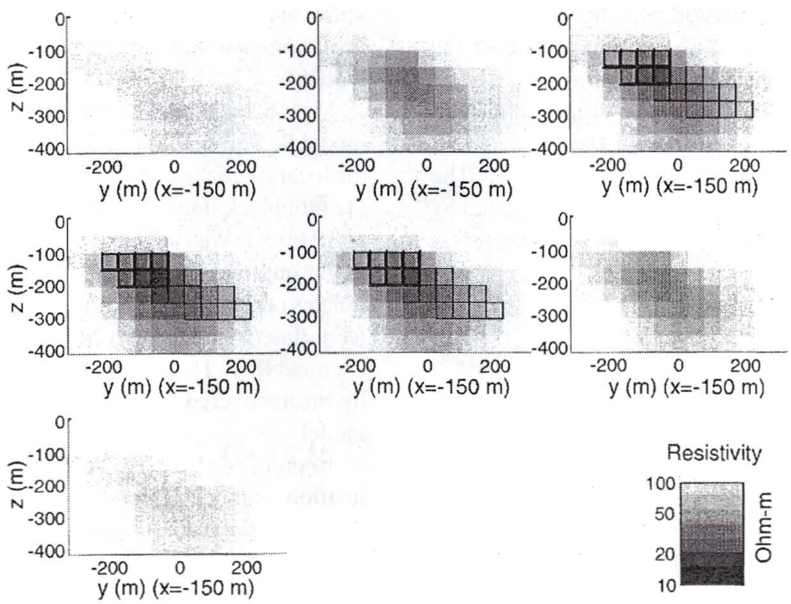

Fig. 6. The resistivity distribution obtained by inversion of the IP data for model 2. Each panel shows the vertical cross sections of the resulting resistivity model along the observational profiles. The bold black lines in these images outline the location of the dipping dike with the IP effect, while the thin black lines outline the conductive part without the IP effect.

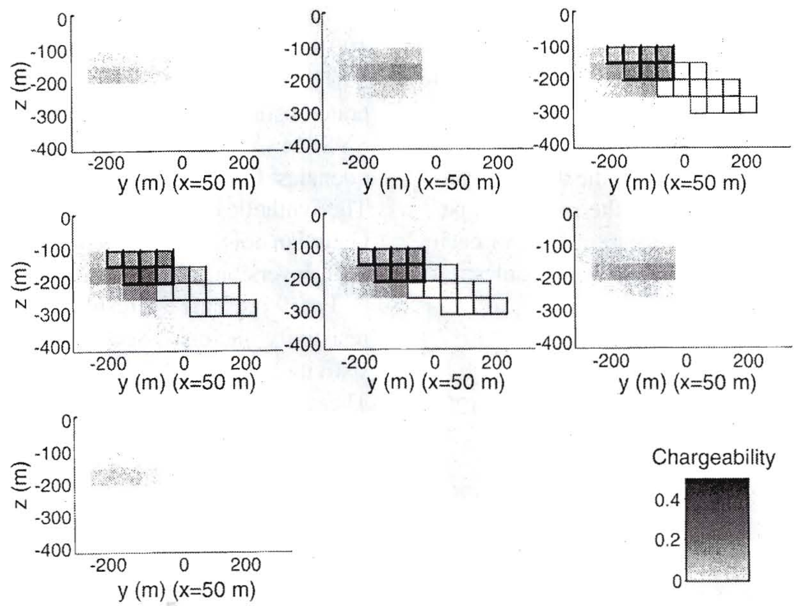

Fig. 7. The chargeability distribution obtained by inversion of the IP data for model 2. Each panel shows the vertical cross sections of the resulting chargeability model along the observational profiles. The bold black lines in these images outline the location of the dipping dike with the IP effect, while the thin black lines outline the conductive part without the IP effect.

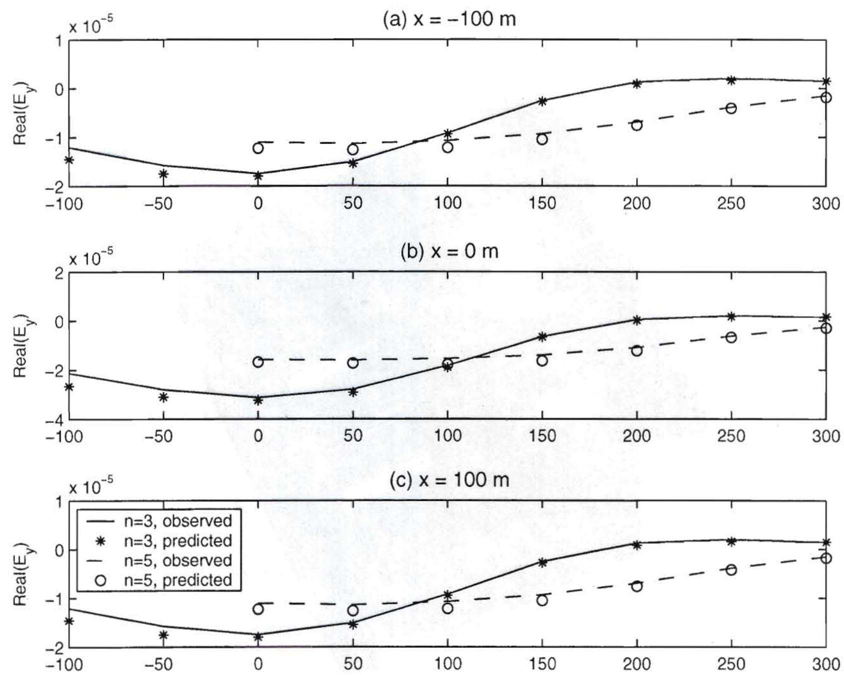

Fig. 8. Plots of a real part of the observed electric field at a frequency of 4 Hz along three profiles passing over the conductive dike. The plots are drawn for the receivers located at the distance of *na* from the end of the bipole transmitter, respectively, where $n = 3$, 5, and $a = 50$ m. The solid lines present the observed data for $n = 3$, while the dashed lines show the observed data for $n = 5$. The stars and circles present the theoretical predicted data computed by the rigorous IE forward modeling code for the model of the dike, obtained by LQL inversion.

slightly at the left part of the profile, where the top of the dike appears more close to the surface of observations.

Model 3 has a similar geometrical structure as model 1 (Fig. 2). However, it represents two conductive bodies in a 100 Ω m homogeneous background with the same resistivity and chargeability, but with the different values of the time parameter τ and of the relaxation parameter C. The Cole–Cole model parameters for each body are defined according to the following tables:

Body 1

$$\begin{aligned} &\rho = 2\,\Omega\,\mathrm{m} \\ &\eta = 0.5 \\ &\tau = 0.4\,\mathrm{s} \\ &C = 0.8 \end{aligned} \tag{20}$$

Body 2

$$\begin{aligned} &\rho = 2\,\Omega\,\mathrm{m} \\ &\eta = 0.5 \\ &\tau = 0.04\,\mathrm{s} \\ &C = 0.3 \end{aligned} \tag{21}$$

The top of the cubic bodies are located at a depth of 100 m. The cubic body sides have a length of 150 m.

The synthetic EM data for this model were generated using integral equation forward modeling code SYSEM (Xiong, 1992). In this case, we used ten frequencies: 0.125, 0.25, 0.5, 1, 2, 4, 8, 16, 32 and 64 Hz. The synthetic observed data were contaminated by 2% Gaussian noise and inverted using focusing regularized LQL inversion.

Fig. 9 presents the result of the inversion for the dc resistivity, the cross sections of the reconstructed resistivity. Fig. 10 shows the recovered charge-ability. The distribution of the time parameter, τ, is shown in Fig. 11, while Fig. 12 presents the distribution of the relaxation parameter C. One can see that the inversion produces good images of the resistivity and chargeability distributions, and of the time and the relaxation parameters of the Cole–Cole model. These parameters may be used for the discrimination of the different types of mineralization, which is an important goal in mineral exploration (Zonge and Wynn, 1975).

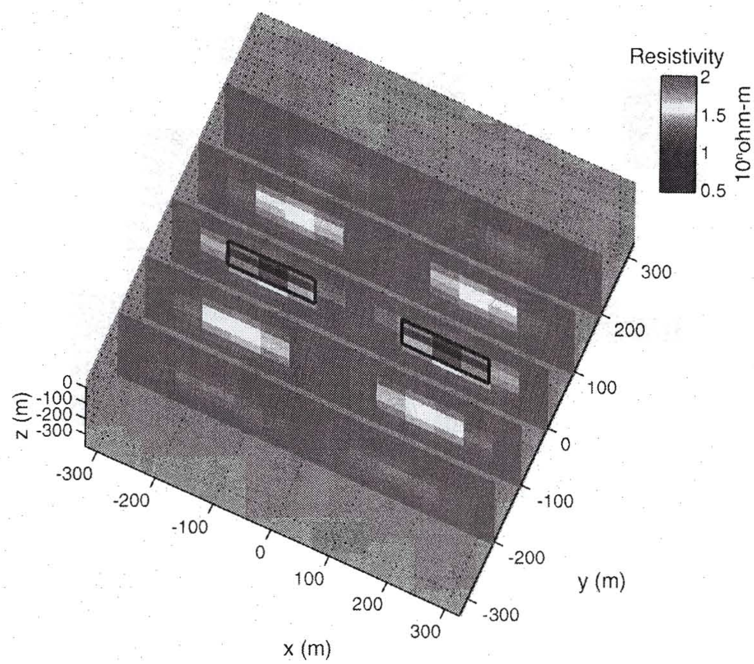

Fig. 9. The resistivity distribution obtained by inversion of the IP data for model 3. The vertical cross sections are perpendicular to the observational profiles. The solid lines outline the true position of the bodies.

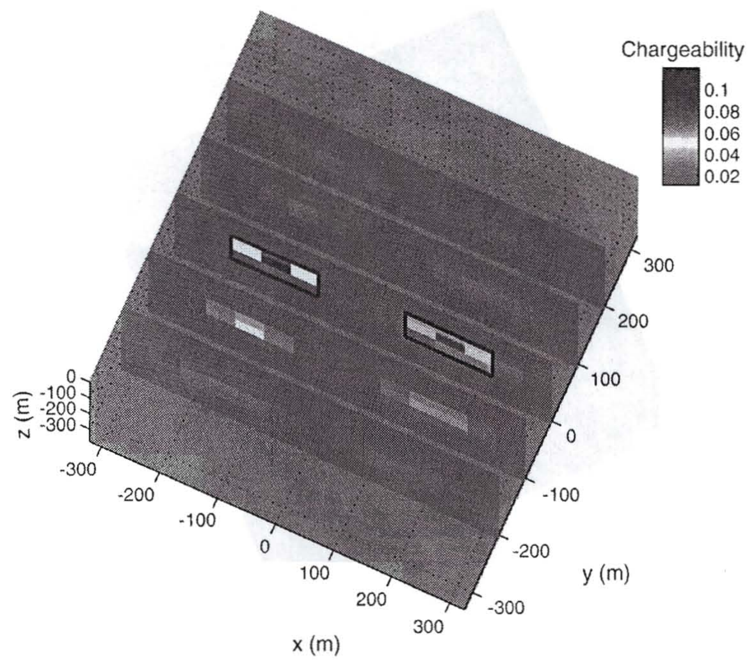

Fig. 10. The chargeability distribution obtained by inversionof the IP data for model 3. The vertical cross sections are perpendicular to the observational profiles. The solid lines outline the true position of the bodies.

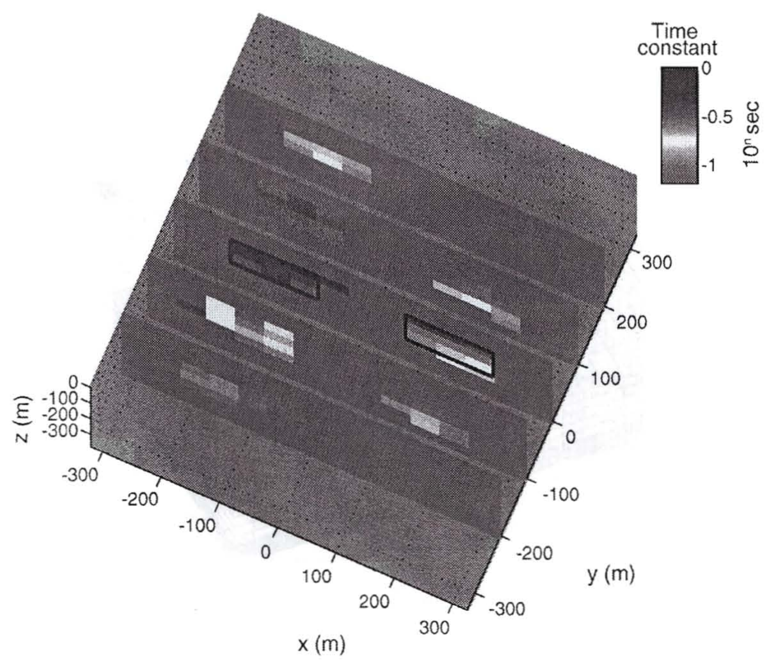

Fig. 11. The time parameter τ distribution obtained by inversion of the IP data for model 3. The solid lines outline the true position of the bodies.

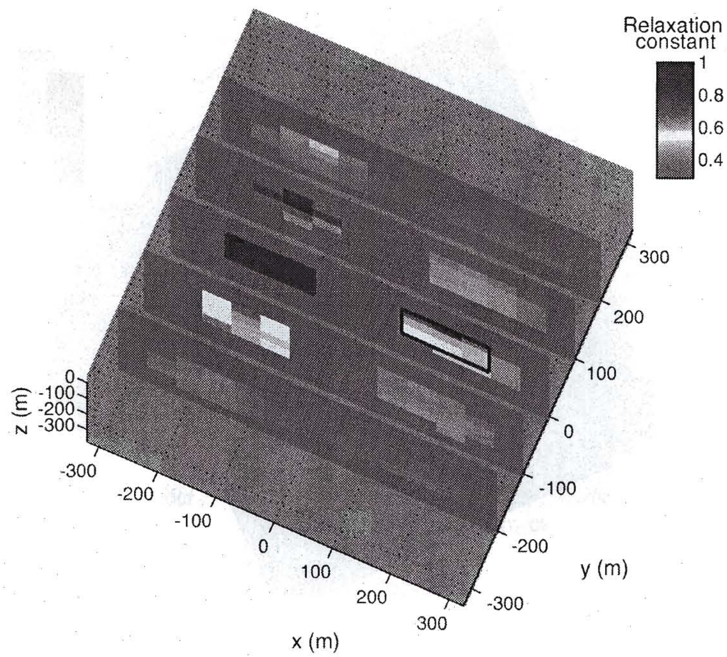

Fig. 12. The relaxation parameter C distribution obtained by inversion of the IP data for model 3. The solid lines outline the true position of the bodies.

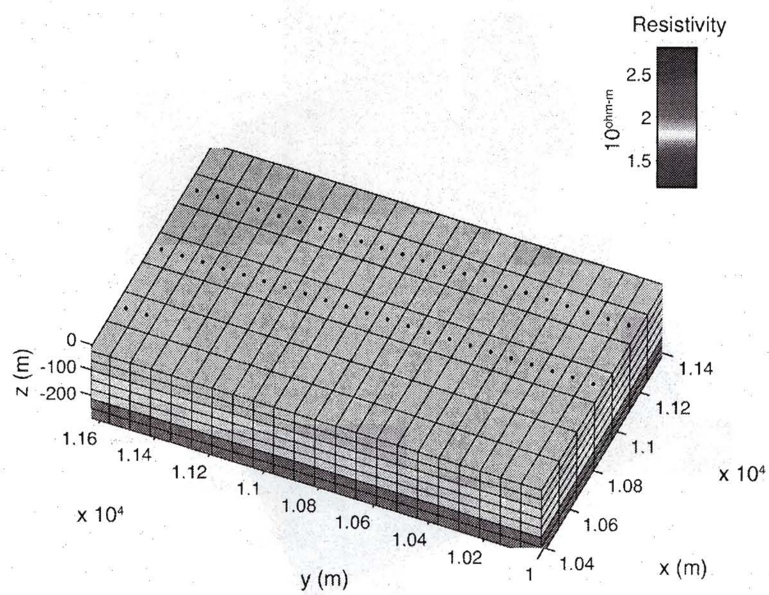

Fig. 13. Three-dimensional sketch of an area of the inversion and the distribution of the survey lines. The black dots on the surface denote the centers of the transmitter and receiver dipoles, respectively. The size of the area is 1050 m × 1650 m × 265.5 m divided by 7 × 22 × 7 cells (in the x, y, and z-directions, respectively).

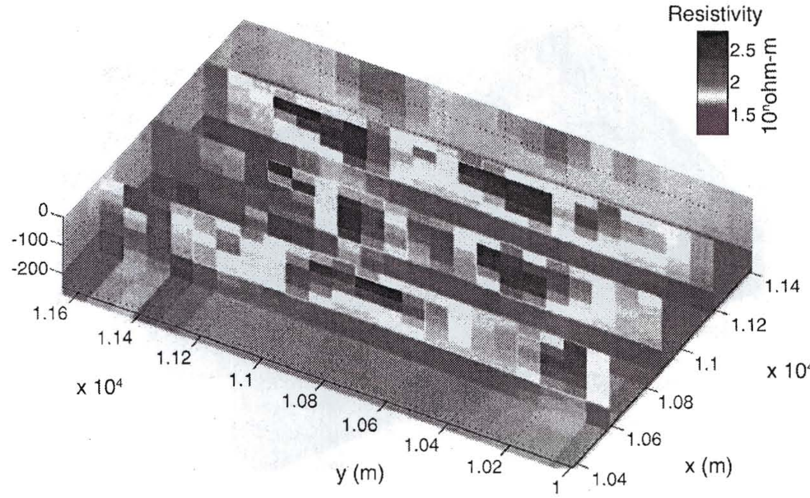

Fig. 14. The vertical cross sections along the observational profiles of the 3D resistivity model computed by LQL IP inversion of the practical IP data.

5. Interpretation of the practical 3D IP data collected by Rio Tinto Mining and Exploration

We have applied our inversion method to real IP data, provided by Rio Tinto Mining and Exploration. We analyze three observational profiles. The IP data were collected by the dipole–dipole array with the length of the transmitter and receiver dipoles $a = 75$ m. For each transmitter position we have up to seven receivers located at the distances of na from the end of the dipole transmitter, where $n = 1, 2, \ldots, 7$, respectively. Each profile has 22 receivers and 14 transmitters. The IP data were measured at one frequency, 0.125 Hz, by the an in-house Zonge system. The dc apparent resistivity was also recorded.

Fig. 13 shows the area of the inversion and the distribution of the survey lines. The black dots on the surface denote the centers of the transmitter and

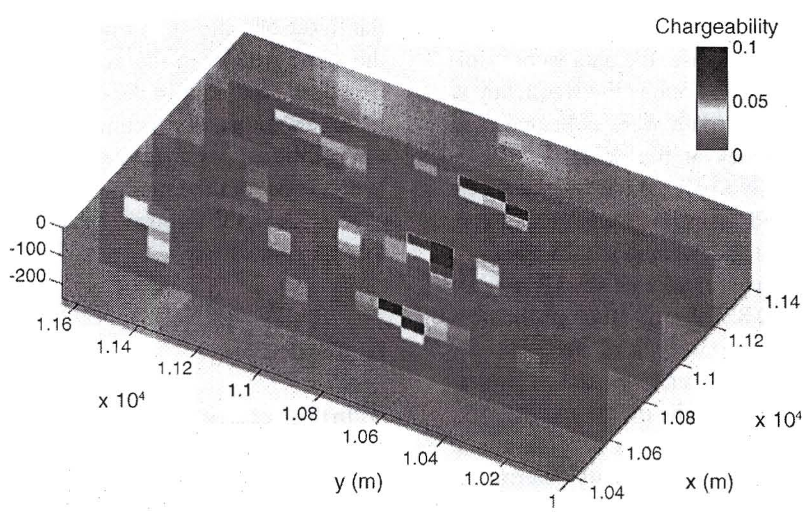

Fig. 15. The vertical cross sections along the observational profiles of the 3D charge-ability model computed by LQL IP inversion of the practical IP data. The relaxation constant C is equal to 0.8.

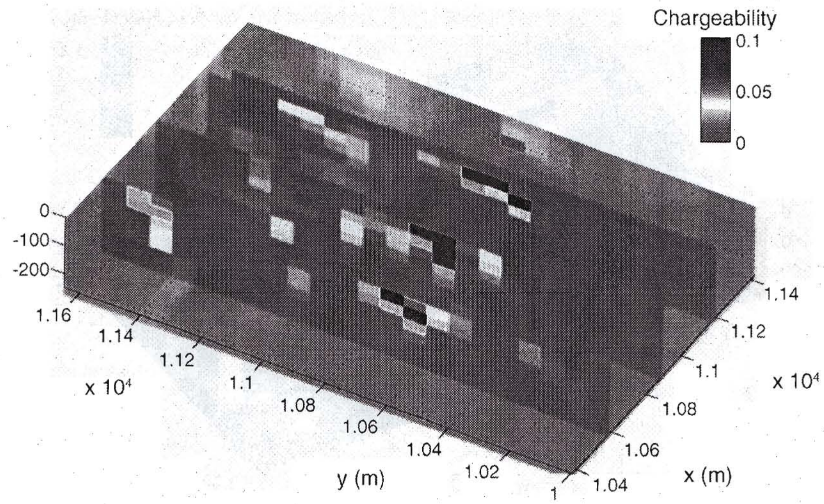

Fig. 16. The vertical cross sections along the observational profiles of the 3D charge-ability model computed by LQL IP inversion of the practical IP data. The relaxation constant C is equal to 0.5.

receiver dipoles, respectively. The size of the area is $1050\,\text{m} \times 1650\,\text{m} \times 265.5\,\text{m}$ divided into $7 \times 22 \times 7$ cells (in the x, y, and z-directions, respectively). First, we applied a standard one-dimensional inversion routine to determine the background resistivity of the model. As a result, we constructed the layered background resistivity model with the following resistivity sequence (from the top to the bottom): 75, 70, 115, 150, 240, and $260\,\Omega\,\text{m}$, and with the following thicknesses of the layers: 80, 110, 150, 190, and 225 m.

Note that in this practical case, the data were available only for two frequencies: one is the frequency at 0.125 Hz, for which the IP data were collected, and the other is zero frequency at the dc limit. Therefore, we may use only two parameters for the inversion: the resistivity, ρ, and the intrinsic chargeability, η. Figs. 14 and 15 present the inversion results obtained for the following fixed parameters of the Cole–Cole model: $\tau = 1$ s and $C = 0.8$. Several other parameters were used as well, and an example of inversion for $C = 0.5$ is shown below. However, the selected parameters provide the best fitting of the observed data.

Fig. 14 presents the vertical cross sections along the observational profiles of the resistivity determined by the inversion, and Fig. 15 shows the inversion result for the chargeability distribution. We can see the spatial images of both the resistivity and chargeability anomalies. We can observe in these images several resistivity anomalies, while there is only one distinguished chargeability anomaly. This result gives us an additional important knowledge about the chargeability distribution, which may benefit the geological interpretation.

For comparison, we run the inversion with a different relaxation parameter, $C = 0.5$. The resulting chargeability distribution is shown in Fig. 16. One can see that the geometry of the chargeability anomaly is similar to the one shown in Fig. 15 and there is practically the same pattern in the anomalous chargeability distribution. Note that in the case of the multi-frequency IP observations, our technique will be able to recover the additional parameters of the Cole–Cole model, as it was shown in the model study. Unfortunately, however, such multi-frequency data was not available for this specific survey.

6. Conclusion

In this paper, we have developed a new technique for 3D simultaneous inversion of electromagnetic data for both electrical conductivity and intrinsic chargeability. This technique is based on the localized quasi-linear (LQL) approximation, which reduces dramatically the computations required for multi-source IP survey modeling and inversion. In contrast to traditional 2D and 3D IP inversion, developed in previous publications (Yuval and Oldenburg, 1997; Routh and Oldenburg, 1998; Li and Oldenburg, 2000), this new method takes into account, though only in an approximate way, the nonlinearity of electromagnetic induction and induced polarization, and allows for the determination of the Cole–Cole model parameters.

The method incorporates both smooth regularized inversion, which generates a smooth image of the inverted conductivity and chargeability, and a focusing regularized inversion, producing a more focused image of the geoelectrical target. The application of the method to synthetic data demonstrates its ability to recover the conductivity and chargeability of resistive and conductive rock formations, as well as the time and relaxation parameters of the corresponding Cole–Cole model.

We have also applied our method to practical IP data collected by Rio Tinto Mining and Exploration for mineral exploration. The result helps to reveal a significant chargeability anomaly in the geological cross-section, which is different from the conductivity anomalies.

Acknowledgments

This work was funded by the National Energy Technology Laboratory of the U.S. Department of Energy under contract DE-FC26-04NT42081. We are thankful to Dr. Steve McIntosh of Rio Tinto Mining and Exploration Ltd. for providing the practical IP data presented in this paper. We also thank Dr. Colin Farquharson and the anonymous reviewer for their useful comments and recommendations which helped to improve the manuscript.

References

Cole, K.S., Cole, R.H., 1941. Dispersion and absorption in dielectrics. J. Chem. Phys. 9, 343–351.

Hohmann, G.W., 1975. Three-dimensional induced polarization and EM modeling. Geophysics 40, 309–324.

Li, Y., Oldenburg, D.W., 1931-1945. 3D inversion of induced polarization data. Geophysics 65.

Pelton, W. H., 1977. Interpretation of induced polarization and resistivity data. Ph.D. Thesis. University of Utah, 255 pp.

Routh, P., Oldenburg, D.W., 1998. Electromagnetic coupling removal from frequency domain IP data in 2D environments: SEG Expanded Abstracts, 68th Ann. Int. Meet., New Orleans.

Seigel, H.O., 1959. Mathematical formulation and type curves for induced polarization. Geophysics 24, 547–565.

Weidelt, P., 1975. EM induction in three-dimensional structures. J. Geophys. 41, 85–109.

Xiong, Z., 1992. EM modeling of three-dimensional structures by the method of system iteration using integral equations. Geophysics 57, 1556–1561.

Yuval, Oldenburg, D.W., 1997. Computation of Cole–Cole parameters from IP data. Geophysics 62, 436–448.

Zhdanov, M.S., Fang, S., 1996a. Quasi-linear approximation in 3D EM modelling. Geophysics 61, 646–665.

Zhdanov, M.S., Fang, S., 1996b. 3D quasi-linear electromagnetic inversion. Radio Sci. 31, 741–754.

Zhdanov, M.S., Fang, S., 1999. 3D quasi-linear electromagnetic modelling and inversion. In: Oristaglio, M., Spies, B. (Eds.), Three Dimensional Electromagnetics, Soc. Explor. Geophys. Dev. Ser., pp. 233–255.

Zhdanov, M.S., Tartaras, E., 2002. Three-dimensional inversion of multi-transmitters electromagnetic data based on the localized quasi-linear approximation. Geophys. J. Int. 148, 506–519.

Zhdanov, M.S., 2002. Geophysical Inverse Theory and Regularization Problems. Elsevier, New York, 628 pp.

Zonge, K., Wynn, J.C., 1975. Recent advances and applications in complex resistivity measurements. Geophysics 40, 851–864.